Developmental Biology 431 (2017) 336–346

Contents lists available at ScienceDirect

Developmental Biology

journal homepage: www.elsevier.com/locate/developmentalbiology

Evolution of developmental control mechanisms

Characterization of *NvLWamide-like* neurons reveals stereotypy in *Nematostella* nerve net development

Jamie A. Havrilak[a], Dylan Faltine-Gonzalez[a], Yiling Wen[b], Daniella Fodera[a], Ayanna C. Simpson[b], Craig R. Magie[b], Michael J. Layden[a,*]

[a] *Lehigh University, Department of Biological Sciences, United States*
[b] *Quinnipiac University, Department of Biological Sciences, United States*

ARTICLE INFO

Keywords:
Nematostella
Transgenic
Neurogenesis
Nerve net
LWamide

ABSTRACT

The organization of cnidarian nerve nets is traditionally described as diffuse with randomly arranged neurites that show minimal reproducibility between animals. However, most observations of nerve nets are conducted using cross-reactive antibodies that broadly label neurons, which potentially masks stereotyped patterns produced by individual neuronal subtypes. Additionally, many cnidarians species have overt structures such as a nerve ring, suggesting higher levels of organization and stereotypy exist, but mechanisms that generated that stereotypy are unknown. We previously demonstrated that *NvLWamide-like* is expressed in a small subset of the *Nematostella* nerve net and speculated that observing a few neurons within the developing nerve net would provide a better indication of potential stereotypy. Here we document *NvLWamide-like* expression more systematically. *NvLWamide-like* is initially expressed in the typical neurogenic salt and pepper pattern within the ectoderm at the gastrula stage, and expression expands to include endodermal salt and pepper expression at the planula larval stage. Expression persists in both ectoderm and endoderm in adults. We characterized our *NvLWamide-like::mCherry* transgenic reporter line to visualize neural architecture and found that *NvLWamide-like* is expressed in six neural subtypes identifiable by neural morphology and location. Upon completing development the numbers of neurons in each neural subtype are minimally variable between animals and the projection patterns of each subtype are consistent. Furthermore, between the juvenile polyp and adult stages the number of neurons for each subtype increases. We conclude that development of the *Nematostella* nerve net is stereotyped between individuals. Our data also imply that one aspect of generating adult cnidarian nervous systems is to modify the basic structural architecture generated in the juvenile by increasing neural number proportionally with size.

1. Introduction

Possession of a centralized nervous system (CNS) is a unifying feature of bilaterians (chordates, insects, nematodes, acoels, annelids, mollusks, echinoderms, etc.). Details regarding the origin of bilaterian central nervous systems are still under debate, but most believe an ancestral nerve net preceded the organized condensation of neurons typical of a bilaterian CNS (Arendt et al., 2008; Ghysen, 2003; Hartenstein and Stollewerk, 2015; Watanabe et al., 2009; Galliot et al., 2009). Cnidarians (e.g. jellyfish, corals, anemones, *Hydra,* etc.) represent the sister taxon to the bilaterians, and their nervous systems are comprised of a nerve net wherein neurites emanating from neural soma scattered throughout the body form a “net” encompassing the organism (Dunn et al., 2008; Hejnol et al., 2009; Rentzsch et al., 2016a). The phylogenetic position of cnidarians in relationship to bilaterians, together with the fact that they have a nerve net, puts this group in a unique position to inform and potentially test hypotheses about the origin and evolution of bilaterian centralized nervous systems. However, very little is known about the developmental patterning of cnidarian nerve nets, which makes it difficult to compare components of cnidarian nerve nets to their putative bilaterian counterparts. In particular, it isn't clear if stereotypical development of cnidarian nerve nets occurs. Thus, determining the stereotypy of nerve net development and identifying distinct neural subtype markers is important to then assess how nerve nets are patterned.

Nerve nets are considered to be the most ancestral and simplest nervous system organization. Herein we refer to the term “organized” to mean having a distinct pattern with systematically arranged and reproducible neurite projections. As recently as 2015 nerve nets were described as “an irregular arrangement of neurites from monopolar,

* Correspondence to: Lehigh University, Department of Biological Sciences, 111 Research Drive, Iacocca Hall Rm B-217, Bethlehem, PA 18015, United States.
E-mail address: layden@lehigh.edu (M.J. Layden).

http://dx.doi.org/10.1016/j.ydbio.2017.08.028
Received 12 April 2017; Received in revised form 25 July 2017; Accepted 25 August 2017
Available online 06 September 2017

bipolar and multipolar neurons" (Hejnol and Rentzsch, 2015). However, a number of observations suggest cnidarian nerve nets are more reproducible than usually appreciated. First, there are obvious structures identified in many cnidarian nervous systems. For example, the sea anemone *Nematostella vectensis* has clearly visible longitudinal tracts that run the length of the oral-aboral axis and are stereotypically positioned over each mesentery structure (Layden et al., 2016b; Marlow et al., 2009; Nakanishi et al., 2012; Rentzsch et al., 2016a). In *Hydra* non-overlapping neural networks have been linked to specific behaviors, which indicates unique functions are assigned to restricted subsets of the nerve net (Dupre and Yuste, 2017). There are distinct subsets of neurons with particular spatial locations that are identifiable in *Hydra* and *Nematostella* (Anderson et al., 2004; Grimmelikhuijzen and Spencer, 1984; Koizumi et al., 2004; Marlow et al., 2009). A nerve ring containing at least 4 different neuronal subsets has been identified at the base of tentacles in *Hydra oligactis* and thought to be involved in feeding behaviors (Koizumi et al., 2015). Two marginal nerve rings have been identified in the jellyfish *Aglantha* (Donaldson et al., 1980; Mackie, 2004; Roberts and Mackie, 1980). Hydrozoan nerve rings are visualized with various different antibodies that do not overlap/colocalize, suggesting that distinct neuronal subpopulations populate the nerve ring, although the number of neurons within and organization of these subpopulations is not clear (Koizumi et al., 2015). Altogether, these observations across many cnidarian species hint at more structural organization within a typical cnidarian nerve net than once thought. One remaining question is whether there is a predetermined pattern to this organization that arises during development.

The sea anemone *Nematostella vectensis* is an anthozoan cnidarian model system that has grown in popularity due to its ease of culture and the ever-growing repertoire of genomic tools available (Darling et al., 2005; Layden et al., 2016b; Putnam et al., 2007). While many cnidarians posses both ectodermal and endodermal nerve nets, the developmental origins of the nervous systems varies between species. In *Nematostella*, neurogenesis occurs in both the ectoderm and endoderm (Nakanishi et al., 2012). Studies primarily conducted in *Nematostella* suggest that cnidarian and bilaterian neural patterning likely share a common evolutionary origin. (Layden et al., 2016b; Rentzsch et al., 2016b). For instance, MEK/MAPK (Layden et al., 2016a), Wnt (Leclère et al., 2016; Marlow et al., 2013; Sinigaglia et al., 2015), BMP (Saina et al., 2009; Watanabe et al., 2014) and Notch (Layden and Martindale, 2014; Richards and Rentzsch, 2015), all key regulators of bilaterian neurogenesis, have similar roles in *Nematostella*. Additionally, key neurogenic transcription factors such as *NvsoxB(2)* and *Nvath-like* are expressed in proliferating neural progenitor cells (Richards and Rentzsch, 2015, 2014). The bHLH proneural transcription factor *NvashA* is necessary and sufficient to promote neurogenesis, including the formation of individual neuronal subtypes (Layden et al., 2012). It has been suggested that the conserved neurogenic programs described above coordinate with axial patterning to generate distinct neural subtypes, similar to mechanisms that pattern bilaterian central nervous systems (Layden et al., 2012; Leclère et al., 2016; Rentzsch et al., 2008; Watanabe et al., 2014). However, an understanding of cnidarian neural architecture or the patterning of distinct neural subtypes in these organisms is lacking, and thus with few exceptions there are not clear neural subtypes that can be used to screen for neural patterning defects.

Our previous efforts identified that the *NvLWamide-like::mCherry* transgenic line labels only a few distinct neural subtypes (Layden et al., 2016a), enabling us to follow the development of individual neurons and quantify the number of neurons of each subtype. We speculated that the neural number and neurite projection patterns were consistent from animal to animal, which if true would suggest the development of nerve nets is at least in some cases stereotyped. Here we characterize the *NvLWamide-like::mCherry* transgenic line to determine how reproducible the development and neurite patterns of a subset of the juvenile and adult nervous system are. We identified at least six neuronal subtypes containing NvLWamide-like::mCherry expression that are consistently found at particular locations in the polyp and with distinct neurite morphologies. By the juvenile polyp stage the number of each neural class is predictable from animal to animal and these subtypes persist through adult stages. Interestingly, the number of neurons for each individual neuronal subtype increases with age, and can in some cases be easily quantified revealing a positive correlation between neural number and body length. These combined data imply that the *Nematostella* nervous system develops and is modified in a stereotypical fashion, which contradicts the notion that nerve nets are loosely organized structures.

2. Materials and methods

2.1. Animal care

All animals were maintained in 1/3 × artificial seawater (ASW) with a pH of 8.1–8.2, with weekly water changes. Embryos were either grown at 25 °C, 22 °C or 17 °C to the desired stages, and juvenile polyps were maintained at room temperature in the dark. Adult *Nematostella* were housed in the dark at 17 °C, were fed brine shrimp 4 times a week, and were given pieces of oyster 1 week prior to spawning. Spawning was induced by changing the light cycle (Fritzenwanker and Technau, 2002; Hand and Uhlinger, 1992). Generation of *NvLwamide-like::mCherry* transgenic animals was described by Layden et al. (2016a). All transgenic animals were from a stable F1 line, and since there was no visible difference in mCherry expression in heterozygous versus homozygous animals both were utilized in these studies.

2.2. In situ hybridization and immunohistochemistry

Protocols for fixation, *in situ* probe synthesis, and both immunohistochemical or double fluorescent *in situ* hybridization were performed as previously described (Wolenski et al., 2013). The *NvLWamide-like* probe was previously described (Layden et al., 2012). The mCherry probe was amplified using the following primers: mCherry Forward: 5′ gcaagggcgaggaggacaac 3′; mCherry Reverse: 5′ cttgtacagctcgtccatgccg 3′. Cloning and probe synthesis were carried out as previously described (Wolenski et al., 2013).

Immuno-staining was performed as previously described (Nakanishi et al., 2012; Wolenski et al., 2013) with the following modifications. Incubations in primary and secondary antibodies were done overnight at 4 °C. Anti-DsRed (Clontech Living Colors DsRed Polyclonal Antibody, 632496, Antibody registry ID: AB_10013483) was diluted 1:100 in blocking reagent (4% goat serum in PBS + 0.2% Triton X-100 + 1% BSA). Secondary Alexa Fluor 555 antibody (Thermo Fisher Scientific, A21428) was used at 1:500 in 1 × blocking reagent.

TUNEL assays were performed using the Click-iT Plus TUNEL Assay kit from ThermoFisher Scientific (C10617) with modifications made for whole mount preparations. Embryos were fixed in 4% paraformaldehyde in 1/3X artificial sea water for one hour, then washed four times in PBS with 1% tween-20 (PTw). Fixed gastrula and early planula stages were then permeabilized using 0.01 mg/mL of proteinase K for five minutes and seven minutes, respectively. The samples were then washed with 2 mg/mL glycine in PTw, washed in PTw, and then refixed in 4% paraformaldehyde in PTw. Positive controls were obtained by treating the samples with DNAse, as stated by the manufacturer protocol, with an extension of the treatment time to one hour to compensate for the increased tissue. DNAse treatment was stopped with four washes of PTw. The manufacturer's protocol was then followed with exception of extending the developing reaction to one hour and stopped by washing in PTw. The samples were treated with 1:10,000 of Hoescht (ThermoFisher Scientific, H3570) and cleared in 90% glycerol.

2.3. Quantification of mCherry/dsred and NvLWamide-like positive cells

To quantify the number of *mCherry*/α–dsRed positive cells that colabel with *NvLWamide-like* positive cells the embryos were mounted to capture z-stacks of lateral views with a 1 μm step size using a Zeiss LSM 880 (Carl Ziess) confocal microscope. Cells were then scored as single or double positive using the Imaris (Bitplane) imaging software.

2.4. Quantification of NvLWanide-like::mCherry-expressing neurons

Juvenile polyps were relaxed in 7.14% (wt/vol) $MgCl_2$ in 1/3 X ASW for 10 min at room temperature. Animals were either examined and quantified live, subjected to live imaging, or imaged following a light fixation and phalloidin stain. Animals were fixed in 4% paraformaldehyde and 0.2% glutaraldehyde (in 1/3 × ASW) for 1 min, followed by fixation in 4% paraformaldehyde (in 1/3 × ASW) for 10–20 min at room temperature on a rocker. Animals were either then washed quickly in PTw and imaged immediately, or washed with PBS + 0.2% Triton X-100 then stained with Alexa Fluor 488 phalloidin (Life Technologies, A12379, 3:200) and mounted in 90% glycerol for immediate imaging.

2.5. Imaging

DIC images of *in situ* hybridization, and live images of NvLWamide-like::mCherry-expression in juvenile polyps and adult *Nematostella* were taken on a Nikon NTi with a Nikon DS-Ri2 color camera and the Elements software (Nikon). Confocal images of live and fixed/stained *Nematostella* NvLWamide-like::mCherry expression in embryos and juvenile polyps were obtained using a Zeiss LSM 880 with LSM Zen software (Carl Ziess) or a Nikon C1 with EZ-C1 software (Nikon). Confocal images were processed using Imaris 8.2 software (Bitplane LLC) and 3D images were constructed from a composite of serial optical sections (z-stacks). Final images were cropped using Illustrator and/or Photoshop (Adobe Inc.).

3. Results

3.1. NvLWamide-like expression is scattered throughout the ectoderm and endoderm during development

NvLWamide-like is expressed in a subset of the nervous system, but its detailed spatiotemporal distribution has not been described (Layden et al., 2012). We used mRNA *in situ* hybridization to better characterize expression of *NvLWamide-like* during development (Fig. 1). *NvLWamide-like* mRNA was first detected in a scattered pattern in the aboral hemisphere of the embryonic ectoderm at the early gastrula stage (Fig. 1A), which recapitulated the previously published gastrula expression pattern (Layden et al., 2012). The ectodermal expression is detected throughout development (Fig. 1B-E, black arrowheads), but the distribution of cells is dynamic. For example, there was a notable decrease in the number of *NvLWamide-like* expressing cells in the aboral ectoderm between the late gastrula and planula stages (compare Fig. 1A and B). Also during planula development ectodermal expression extends orally and can be detected in the developing pharynx (Fig. 1B and C, white arrowheads). By juvenile polyp stage, ectodermal *NvLWamide-like* expression is detected throughout the entire ectodermal body column and in the tentacles (Fig. 1D-E).

NvLWamide-like is also expressed in small number of endodermal cells. Endodermal expression is first detected in early planula stage animals (Fig. 1C, yellow arrowhead). Endodermal expression is main-

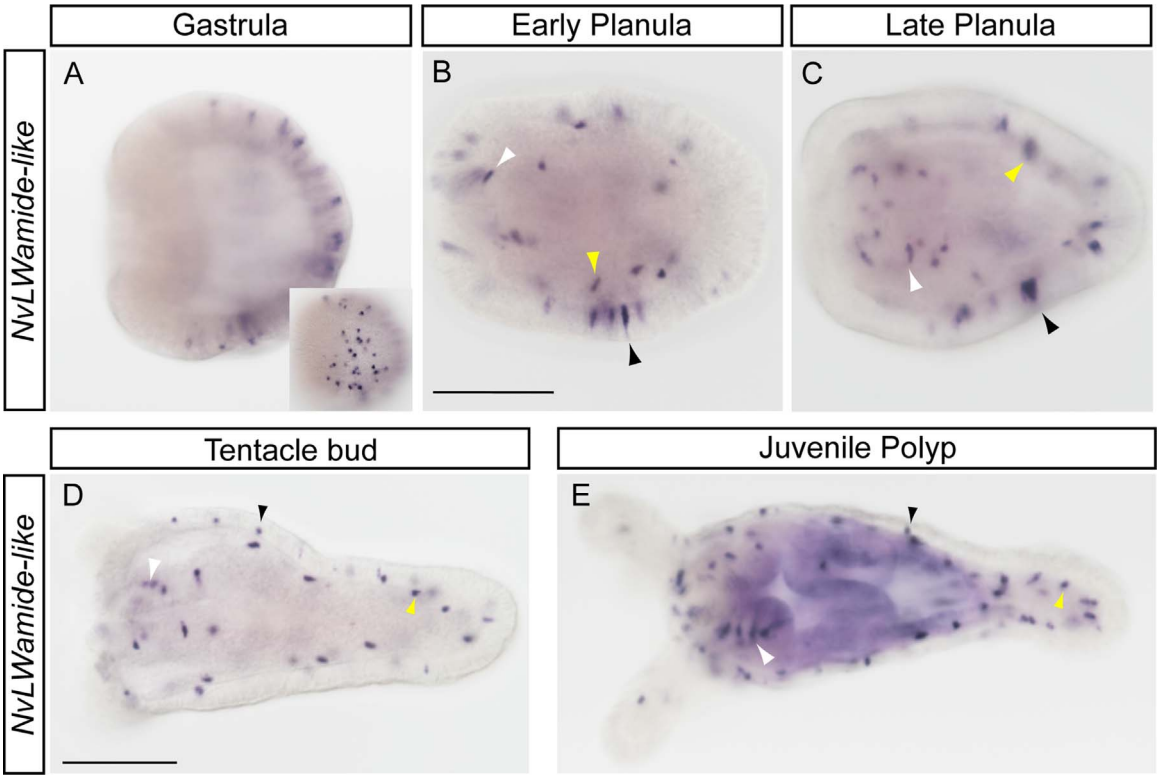

Fig. 1. Expression of *NvLWamide-like* during development. (A) *NvLWamide-like* mRNA is first detected in ectodermal cells during the gastrula stage in a salt-and-pepper pattern. (B-E) Salt-and-pepper ectodermal *NvLWamide-like* expression is maintained in the early and late planula (B and C, black arrowheads), tentacle bud polyp (D, black arrowhead) and juvenile polyp (E, black arrowhead). *NvLWamide-like* expression is detected in the presumptive endoderm by the early planula stage (B, yellow arrowhead) and expression is maintained throughout development (C-E, yellow arrowheads). *NvLWamide-like* positive cells are observed in the pharyngeal ectoderm in the early planula stage (B, white arrowhead) and continue to be detected in the pharyngeal region throughout development (C-E, white arrowheads). *NvLWamide-like* cells are also present in the tentacles of juvenile polyps (E). All images are lateral views with the oral end towards the left. Inset is a surface view of the gastrula embryo in A. Scale bars = 100 μm.

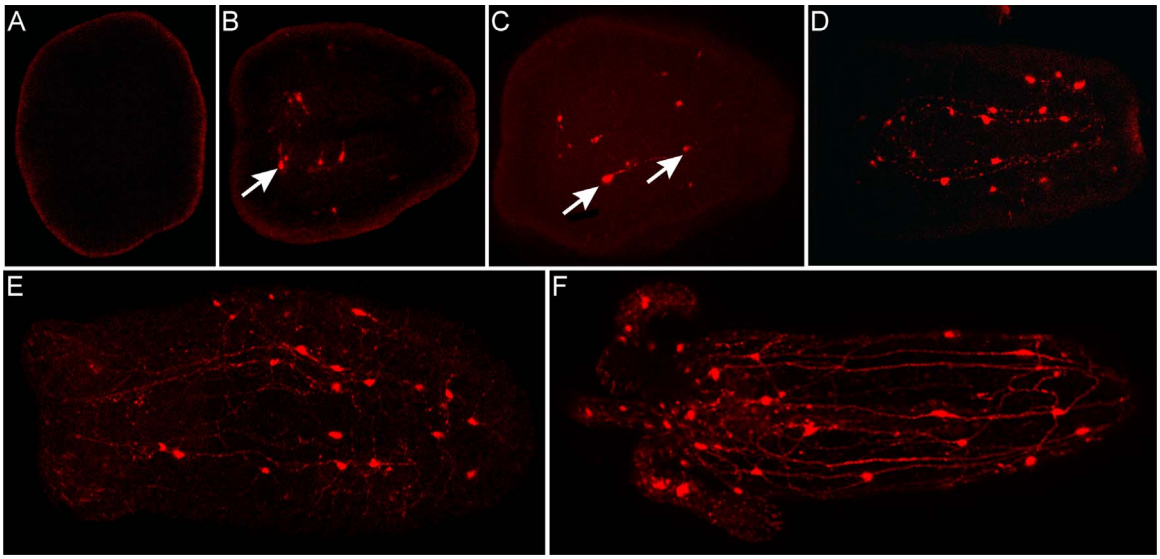

Fig. 2. Visualization of NvLWamide-like::mCherry-expressing neurons during development. (A) NvLWamide-like::mCherry expression is not visible during the gastrula (A) or early planula (not shown) stages of development. (B-C) NvLWamide-like::mCherry positive neurons are first observed in the mid-planula stage, when neurons around the pharynx (arrow in B) and within the ectoderm (arrows in C) become visible. (D) By the late planula stage expression can be seen in the longitudinal neurons (note neurites extending along the oral-aboral axis). (E) By the tentacle bud stage, more numerous lateral connections can be seen between longitudinal neurites. (F) The number of NvLWamide-like::mCherry positive neurons continues to increase into the juvenile polyp stage. Images depict *in vivo* mCherry expression.

tained throughout development (Fig. 1C-E, yellow arrowheads) and into adult stages (see below). Additionally, endodermal cells are associated with the mesenteries and longitudinal tracks that run the length of the oral-aboral axis (Fig. 2D) (Layden et al., 2016b, 2016a; Nakanishi et al., 2012).

3.2. *NvLWamide-like::mCherry expression recapitulates endogenous NvLWamide-like mRNA expression during polyp stages*

To better determine what cell types express *NvLWamide-like,* we generated a stable F1 *NvLWamide-like::mCherry* transgenic reporter line. We found that mCherry expression followed the expression dynamics of the endogenous *NvLWamide-like* transcript (compare Figs. 1 and 2) with the exception that mCherry positive cells are not readily detected in gastrula and early planula stage animals (Fig. 2A). NvLWamide-like::mCherry neurons are first detected in the ectoderm (Fig. 2C, arrows) and in the pharynx of the planula (Fig. 2B, arrow). Tentacular and endodermal expression of mCherry is detected at similar stages to those observed for the endogenous transcript (Fig. 2D-F).

Because of the lack of mCherry transgene expression during early development we wanted to confirm that the *NvLWamide-like::mCherry* transgene faithfully recapitulates *NvLWamide-like* expression. To determine the degree of overlap between endogenous and transgenic *NvLWamide-like* expression we performed fluorescent *in situ* hybridization (FISH) and α–dsRed immunofluorescence to label endogenous *NvLWamide-like* and mCherry protein, respectively. We also performed double FISH to compare endogenous *NvLWamide-like* to *mCherry* transcript co-expression. At gastrula and early planula stages no α–dsRed staining was detected (Fig. 3A and B), consistent with our observation that mCherry is not detected at these stages. α–dsRed was first detected by immunofluorescence in the planula stage and we observed a range from 75% to 100% of α–dsRed positive cells co-expressing *NvLWamide-like* (N = 5 animals, average co-expression = 84.3%) (Fig. 3C), but many *NvLWamide-like* positive cells are still negative for α–dsRed. By polyp stages we observed a range of 80–91% of α–dsRed positive cells co-expressing *NvLWamide-like* (N = 7 animals) (Fig. 3D). We speculated that the observed delay in mCherry co-expression during early stages reflected a delay in mCherry protein maturation rather than a lack of co-expression at early stages. To address this hypothesis, *NvLWamide-like::mCherry* animals were fixed and double fluorescent *in situ* hybridization was performed to label both the endogenous *NvLWamide-like* and the *mCherry* transcript. We were unable to detect *mCherry* in the gastrula stage, but did detect *mCherry* in the early planula stages, and observed that 100% of *mCherry* positive cells co-expressed *NvLWamide-like* (Fig. 3E-G) (N=6 animals). Similarly 100% of *mCherry* positive cells at polyp stages also showed 100% co-expression with *NvLWamide-like* (Fig. 3H-J). Our data suggest that there is a delay in transgene expression compared to the endogenous *NvLWamide-like* expression, and that some of the gastrula *NvLWamide-like* positive cells do not express the transgene. However, by polyp stages there is effectively a 1:1 correlation of *NvLWamide-like* and *mCherry* expression, indicating that our transgene faithfully recapitulates endogenous expression in the mature nervous system.

3.3. *NvLWamide-like::mCherry positive neurons represent distinct neuronal subtypes that develop in a stereotypic manner*

We next characterized the neuronal subtypes that express *NvLWamide-like* during development by analyzing the distribution of and projection patterns present in different NvLWamide-like::mCherry-expressing cells. Initially, twelve day old juvenile polyps were analyzed to determine if the pattern of NvLWamide-like::mCherry expressing neurons were consistent between animals at the end of embryonic and larval development. We were able to identify six neural subtypes that we have assigned the identity of *NvLWamide-like* pharyngeal, -mesentery, -longitudinal, -tentacular, -tripolar, and -quadripolar neurons (Figs. 4–6; Supplemental Figs. 1 and 2; Supplemental movie 1). We also identified mCherry positive nematosomes, which are easiest to observe embedded in the egg mass during spawning (Fig. 6K and L). Eighteen day old (Supplemental Fig. 2A) and twenty three day old (Supplemental Fig. 2B) polyps showed no noticeable increases or decreases in neural number and no additional neural subtypes compared to twelve day old polyps (Compare Supplemental Fig. 2A and B with Figs. 4A and 7A). However, by adult stages the same neural subtypes identified in juvenile polyps were present but were increased in number (Fig. 7). Below we describe each neuronal class in detail. We conclude that the neurons present in the juvenile polyp represent the complement of neurons specified during

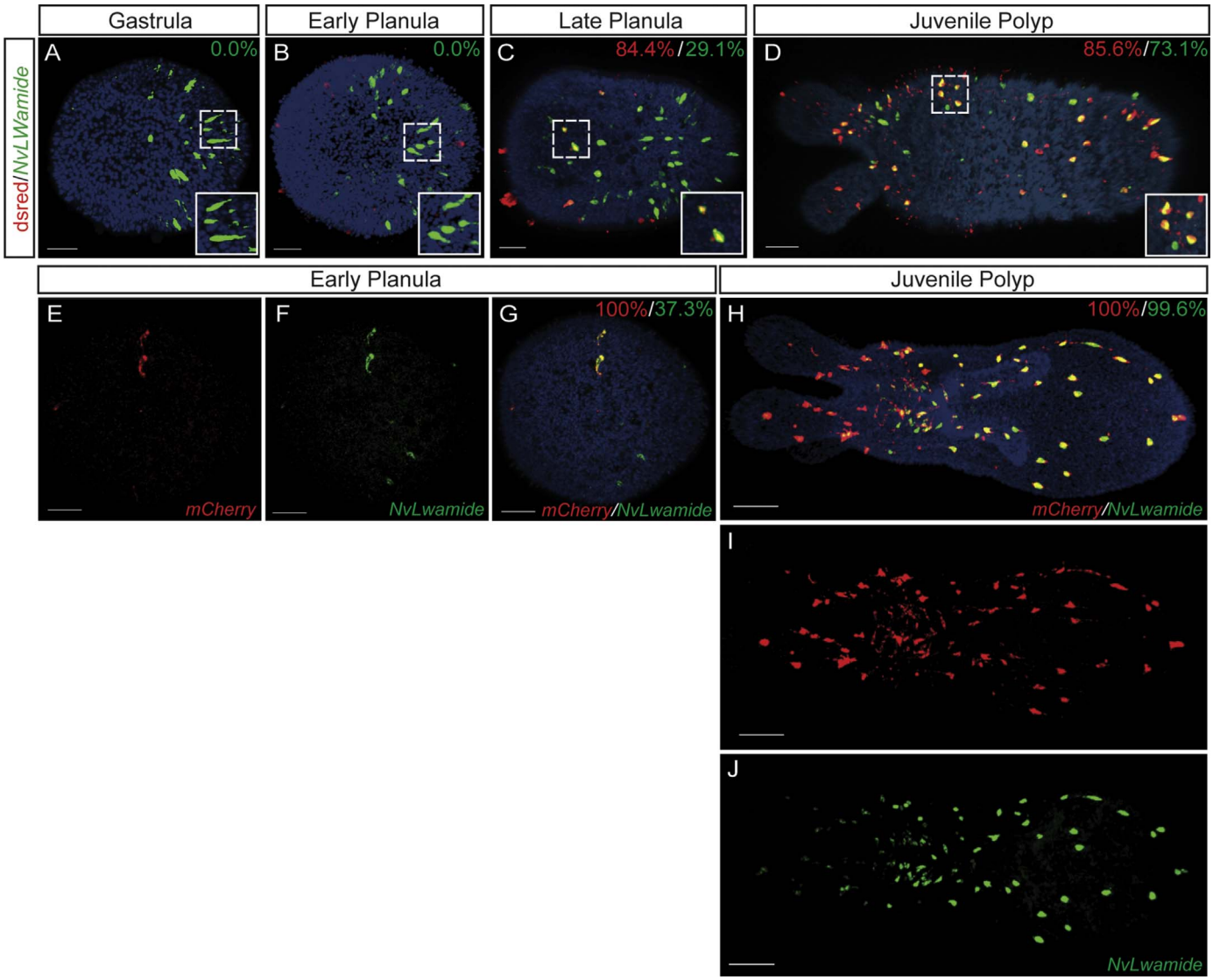

Fig. 3. Colocalization of mCherry transgene with endogenous NvLWamide-like. (A, B) The mCherry transgenic protein, labeled with α-dsred, is not detected during gastrula and early planula stages. (C) By late planula stages 84.3% of the α-dsred positive cells are also *NvLWamide-like* positive (red) while only 29.1% of the *NvLWamide-like* mRNA positive cells are also α-dsred positive (green) (D) At the juvenile polyp stage 85.6% of the α-dsred positive cells are also *NvLWamide-like* mRNA positive (red) while 73.1% of the *NvLWamide-like* mRNA positive cells colabel with α-dsred (green). (E-J) Analysis of the *mCherry* transgenic mRNA showed that 100% of the mCherry positive cells are also *NvLWamide-like* positive at the gastrula stage (E-G) and at the juvenile polyp stage (H-J). Percentages in the top right corners indicate the percentage of α-dsred/*mCherry* positive cells which are also NvLWamide-like positive (red) and the percentage of *NvLWamide-like* mRNA positive cells which are also α-dsred/*mCherry* positive (green). For *NvLWamide-like* mRNA and α-dsred colabeling experiments n = 5, 6, 5, 7 for early gastrula, gastrula, planula, and juvenile polyp respectively. For *NvLWamide-like* and *mCherry* mRNA colabeling experiments n = 6 for gastrula and n = 5 for juvenile polyps. All images are lateral views with the oral end towards the left. Scale bars = 30 μm.

embryonic and larval development, and that additional neurons are not born until after the polyp starts to feed and begins to grow.

3.4. Pharyngeal neurons

NvLWamide-like pharyngeal neural somas are located within the pharyngeal ectoderm (Fig. 4A, orange arrow; Fig. 4B; Fig. 5A, arrowheads). The neurites project out of the basal surface of the soma and encompass/wrap around the pharynx (Fig. 5A and B, arrows). *NvLWamide-like* pharyngeal cell bodies span the pharyngeal ectoderm (Fig. 5A; Supplemental Fig. 1A; Supplemental movie 1) and their apical surface appears to be exposed to the pharyngeal lumen. A view of the basal surface of the *NvLWamide-like* pharyngeal neurons suggests that initially the neurons are formed somewhat in a row (Fig. 5B, arrowhead), each with 2 neurites that project orthogonally to the oral-aboral axis (Fig. 5B, arrow). *NvLWamide-like* neurons contribute to the pharyngeal nerve mesh that surrounds the pharynx in the adult *Nematostella* (Fig. 5C). By adult stages many *NvLWamide-like* pharyngeal neurons are detected throughout the pharynx and they do not appear to be restricted to a particular location. It is difficult to observe pharyngeal neurites in adult animals because the adult pharynx has robust red auto fluorescence. However, the *NvLWamide-like* pharyngeal neurites appear to maintain a mesh around the pharynx and do not appear to condense into a pharyngeal ring, which has been previously hypothesized to exist in *Nematostella* (Marlow et al., 2009). Based on the *NvLWamide-like* mRNA *in situ* and developmental time course in *NvLWamide-like::mCherry* transgenic animals (Figs. 1 and 2) the pharyngeal neurons are born in the pharynx at early planula stages, coincident with or shortly after pharynx formation. Fourteen day old juvenile polyps have an average of 25.9 (+/− 6) NvLWamide-like::mCherry positive neuronal cell bodies in the pharynx (Table 1). This suggests that at while these neurons are present in the pharynx of every animal, their develop-

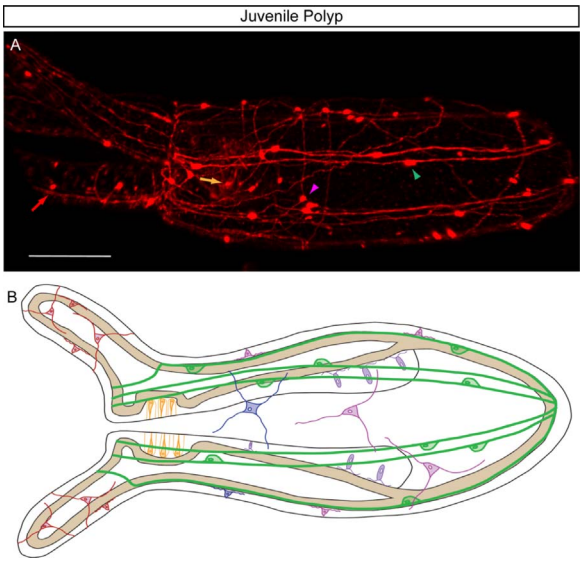

Fig. 4. Overview of NvLWamide-like::mCherry positive neurons. (A) 3D projection of a live confocal image of NvLWamide-like::mCherry expression identifies neurons in the juvenile polyp *in vivo*. Tentacular (red arrow), pharyngeal (orange arrow), tripole (magenta arrowhead), and longitudinal (green arrowhead) neurons are visible in this projection. (B) Schematic of NvLWamide-like::mCherry expressing neural subtypes are depicted as tentacular (red), pharyngeal (orange), quadripolar (blue), tripolar (magenta), longitudinal (green), and mesentery (purple). Oral end is to the left. Scale bar = 50 μm.

ment is not synchronized from animal to animal. As the animal matures and the pharynx increases size the number of pharyngeal neurons also grows.

3.5. Mesentery neurons

NvLWamide-like mesentery neurons are aptly named for their location in the mesentery (Fig. 4B and Fig. 5D-F). Initially the juvenile polyp possesses only a few (between 1 and 4) mesentery neurons (Fig. 5D), with an average of 2.79 (+/− 1.13) *NvLWamide-like* positive neuronal cell bodies per mesentery (Table 1). In feeding adults, however, *NvLWamide-like* mesentery neurons are located along the entire length of the mesentery (Fig. 5E and F, arrowheads; Supplemental Fig. 1C). In adult *Nematostella* the soma seem to be in pairs (Fig. 5E, arrowheads) mirrored on either side of the tract of neurites generated along the mesentery by these neurons (Fig. 5E and F; Supplemental Fig. 1C). We observe both unipolar (a single projection) (Fig. 5F and Supplemental Fig. 1C, arrows) *NvLWamide-like* mesentery neurons and bipolar (two projections that project 180° opposite one another) (Fig. 5F and Supplemental Fig. 1C, arrowheads) *NvLWamide-like* mesentery neurons. The projections emanate from the basal pole and fasciculate into bundles that project along the long axis of the mesentery (Fig. 5F; Supplemental Fig. 1C). Because the tracts of neurites are immediately adjacent to the mesentery neural soma, it is difficult to estimate what percentage of the mesentery neurons are either uni- or bipolar. While we first observe *NvLWamide-like* mesentery neurons in the polyp stage, we speculate that their development occurs earlier, but that the delay in mCherry maturation makes identifying them in larval stages difficult.

3.6. Longitudinal neurons

The longitudinal *NvLWamide-like* neurons are endodermal and organized along the longitudinal neuronal tracts previously described to run above each of the eight mesenteries (Layden et al., 2016b; Nakanishi et al., 2012). The longitudinal tracts divide the body column of the polyp into 8 radial segments that extend the entire length of the oral-aboral axis. Each longitudinal tract has two parallel bundles of fasciculated neurites. The *NvLWamide-like* longitudinal neural somas that reside within these tracts have bipolar projections that originate from the soma 180° to one another (Fig. 4, green arrowhead; Figs. 5G and 5H, yellow arrowheads; Supplemental Fig. 1B). The projections span the entire body length of the animal along the oral-aboral axis. The juvenile polyp usually has 2–3 NvLWamide-like::mCherry positive cell bodies in each of the two parallel tracts present above each mesentery (Fig. 5G), which translates to ~4–6 longitudinal neurons/radial segment (Fig. 7C) with an average of 4.85 +/− 1.01 (Table 1). The mRNA *in situ* and developmental time course data show that longitudinal neurons are born in planula stages and neurites are already projecting prior to the tentacle bud stage (Figs. 1; 2D). Longitudinal neurons show a dramatic increase in cell number in adult animals (Compare Figs. 5G to 5H and 7B to 7A). We quantified the number of longitudinal neurons in a number of animals (Fig. 7C, light grey bars; Supplemental Table 1) and found that the total number of neurons in each tract positively correlates with body length, suggesting that the neuronal number is being controlled relative to the overall body length.

3.7. Tentacular neurons

NvLWamide-like tentacular neurons are first detected shortly after tentacle bud formation (Fig. 4A, red arrow; Fig. 6A). Cell bodies are initially located both in the ectoderm (Fig. 6A and B, white arrowhead) and endoderm (Fig. 6A, yellow arrowhead) and are observed along the entirety of the proximal-distal axis of the tentacle. It is important to note that observing endodermal tentacular neurons is rare. A typical juvenile polyp tentacle has on average ~3 (+/− 1.71) cell bodies per tentacle (Table 1). By adult stages the number of tentacular neurons dramatically increases and nearly all *NvLWamide-like* tentacular neurons are found in the ectoderm. It is unclear whether endodermal neurons migrate into the ectoderm or are lost by adult stages, but to date no trans-tissue layer migration has been described for *Nematostella* neurons. Tentacular neurites project in a fashion that appears to be similar to the tripolar neurons (described below) (Fig. 6B and C).

3.8. Tripolar and quadripolar neurons

The last two subtypes of neurons we identified are the *NvLWamide-like* tripolar and quadripolar neurons. These neurons are named for the number of projections from each soma. Tripolar and quadripolar neurons are found in the ectoderm. The soma for each neural type spans the entire depth of the ectoderm and their cell bodies are reminiscent of previously described sensory neurons (Fig. 6D-J) (Marlow et al., 2009). The projections originate from the basal lateral surface and appear to project within or on the outer surface of the mesoglea. The juvenile polyp has on average at least 1 tripolar neuron per radial segment (1.4 +/− 0.82, Table 1), but we have observed up to 3 neurons per radial segment (Fig. 4A, magenta arrowhead; Fig. 6D; Fig. 7C). The location of tripolar neurons along the oral-aboral axis does not appear to be restricted to a particular region of the body column. At adult stages the number of tripolar neurons increases, and similarly to the longitudinal neurons the increase in tripolar neurons positively correlates with animal length (Fig. 6F and J; Fig. 7C; Supplemental Table 1).

At the early juvenile polyp stage we also sometimes observe *NvLWamide-like* quadripolar neurons (Fig. 6E). Quadripolar neurons have four neurites that emanate from the soma and are similar to the tripolar in that they are located in the ectoderm. When detectable, quadripolar neurons can be first identified as early as 12 days post fertilization (dpf). Interestingly, unlike the tripolar neurons, these neurons appear to be more restricted to the oral portion of polyp trunk. While quadripolar neurons are also observed in the adult (Fig. 6G) their numbers are not significantly increased, and their presence in the adult is difficult to detect.

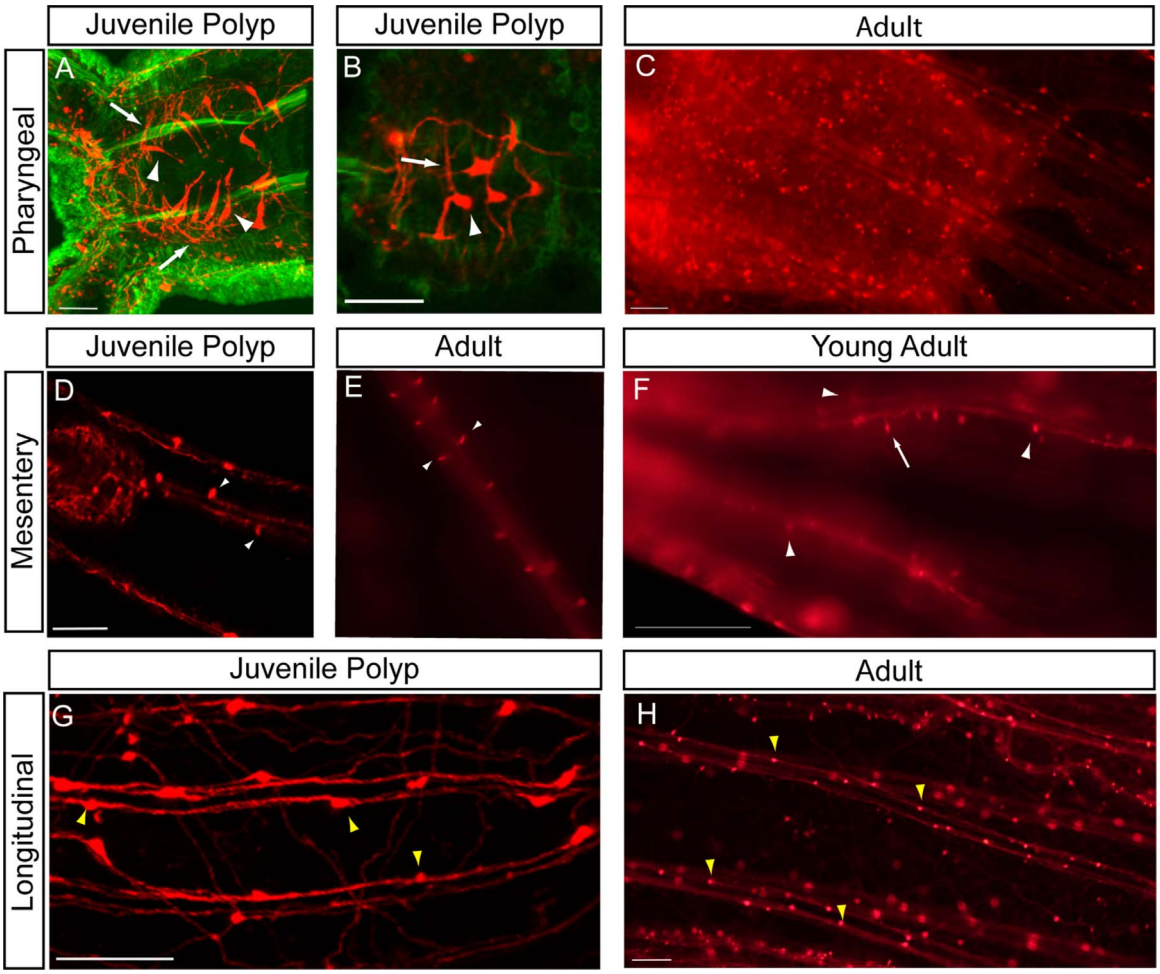

Fig. 5. *NvLWamide-like::mCherry* transgenic line highlights multiple neuronal subtypes. (A-C) NvLWamide-like::mCherry expressing pharyngeal neurons (white arrows and arrowheads) are found in the juvenile polyp (A and B) and the adult (C) and wrap around the pharynx. (D-F) NvLWamide-like::mCherry positive neurons are observed in the mesenteries of both juvenile polyps (D) and adults (E and F). (D) Endodermal focal plane of a lateral view of a juvenile polyp shows mesentery cell bodies (arrowheads). (E) Endodermal view of filleted adult animal demonstrates that mesentery neurons are paired in adults. (F) Endodermal focal plane of a lateral view of an adult animal shows increased mesentery neurons, including unipolar (arrow) and bipolar (arrowhead) neurons. (G and H) Longitudinal neurons (yellow arrowheads) are located in the endoderm and run in 2 parallel lines that follow the mesentery tracts in both juvenile polyps (G) and adults (H). The juvenile polyp shown in A and B was lightly fixed and co-stained with phalloidin (green), with *in vivo* mCherry expression in red. C-H represent *in vivo* images of mCherry expression (red) in live animals. In all images the oral end is to the left. Scale bars = 20 μm (A and B), 50 μm (D and G) and 100 μm (C, F, and H).

In the juvenile polyps, quadripolar neurons were observed in 23% of the radial segments that we quantified (an average of 0.23 +/− 0.43 cells per radial segment) (Table 1). We characterized the tripolar and quadripolar neurons separately because they are morphologically different. However, we cannot rule out that tripolar and quadripolar neurons are the same neural subtype and that there is some variability in the number of projections, with three being significantly more common. If they are in fact the same subtype, the average number of these tri/quad polar neurons increases to an average of 1.63 (+/− 0.95) per radial segment (Table 1).

We currently suspect that the tripolar and quadripolar neurons are the first neural cell types born at gastrula stages, as that is the time we observe the most nascent ectodermal expression of *NvLWamide-like* (Fig. 1). Interestingly the number of *NvLWamide-like+* ectodermal cells decreases after the gastrula stage, suggesting that tripolar/quadripolar cells might be initially specified in excess and some of those cells undergo apoptosis. However, we did not observe any TUNEL positive *NvLWamide-like* positive cells at gastrula and early planula stages (Supplemental Fig. 3). The lack of TUNEL staining suggests that *NvLWamide-like+* cells may be changing fates or losing expression of *NvLWamide-like* throughout development. Previous reports indicate that patterning in the aboral region where *NvLWamide-like* cells first arise is highly dynamic (Leclère et al., 2016; Rentzsch et al., 2008; Sinigaglia et al., 2013), supporting potential shifts in fate. However, to date our data do not allow exclusion of either hypothesis.

3.9. *NvLWamide-like::mCherry is expressed in nematosomes*

Nematosomes are a *Nematostella* specific feature, comprised of a collection of both cnidocyte (stinging) cells and non-cnidocyte cells whose identity is unclear (Babonis et al., 2016). We detect NvLWamide-like::mCherry expression in the nematosomes along the entire length of the tentacle lumen (data not shown), in the nematosomes harvested from an egg mass (Fig. 6K and L), and moving throughout the gut cavity of the polyp (not shown). Even though we did not detect nematosomes via mRNA *in situ,* previous reports detected *NvLWamide-like* expression in nematosomes by RNAseq analysis (Babonis et al., 2016).

4. Summary of results

Our observations support stereotypy in the development of the *Nematostella* nerve net. The juvenile polyp contains specific subtypes of *NvLWamide-like* positive neurons, whose position and neurite projection patterns show minimal variation from animal to animal.

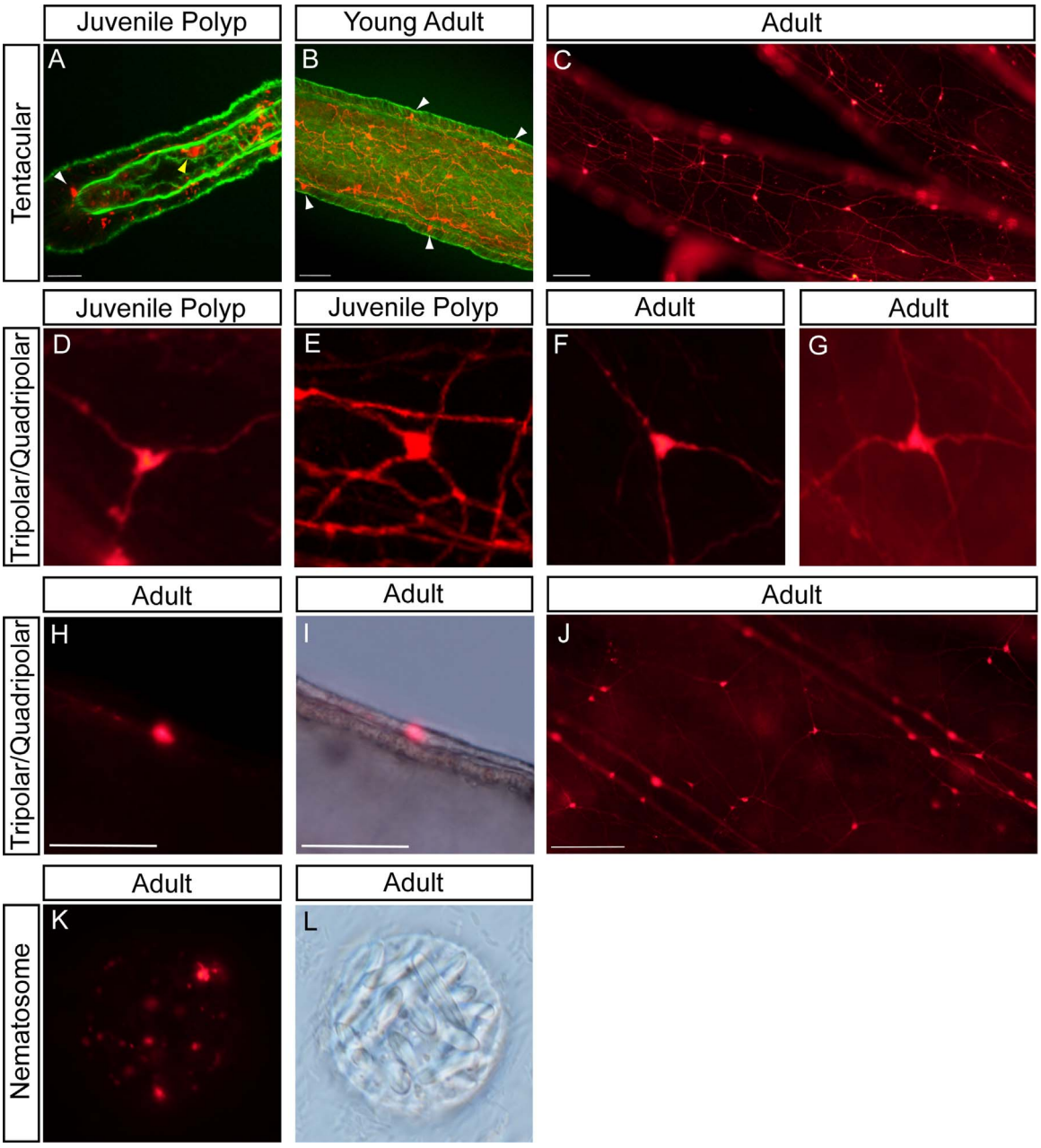

Fig. 6. Ectodermal neuronal subtypes identified by *NvLWamide-like::mCherry* transgenic line. (A-C) Ectodermal NvLWamide-like::mCherry expressing tentacular neurons (white arrowheads) are observed in the basal ectoderm of the juvenile polyp (A), young adult (B) and adult (C). Neurons are located basally with projections that extend to other cell bodies (B and C) and appear to form a network of tripolar neurons (C). *NvLWamide-like* tentacular neurons have a sensory neuron morphology (B). Endodermal *NvLWamide-like* tentacular neurons are also found in the juvenile polyp (A, yellow arrowhead). (D-J) Neurons with a tripolar and quadripolar morphology are located throughout the entire ectodermal body column. Tripolar neurons have 3 projections and are present in both the juvenile polyps (D) and adults (F, H-J). Quadripolar neurons have 4 neurite projections and are present in juvenile polyps (E) and adults (G). Lateral view of an mCherry expressing tripolar neuron (H). Same view and neuron as in H with DIC overlay, showing neuron is located in the ectoderm (I). By the adult stage a network of tripolar and quadripolar neurons is observed (J). (K-L) NvLWamide-like::mcherry expression is detected in the nematosomes (K). DIC image of K showing the structure of the nematosome (L). Samples in A and B were lightly fixed and co-stainied with phalloidin (green), which highlights F actin filaments. C-L portray *in vivo* expression of mCherry captured in live animals. Scale bars = 20 μm (A), 50 μm (B, H-I) and 100 μm (C and J).

Additionally, the number of neurons present for each neuronal subtype are consistent between individuals at the end of development. These data argue that although the nerve net appears unstructured when viewed in its entirety, it is comprised of individual neural subtypes. Furthermore, we found that development of these subtypes is stereotyped, suggesting that the neurite projection patterns for each neural subtype are predetermined. Our data imply that the neural cell types patterned during embryonic and larval development pioneer the neurite architecture present in the adult animal. During adult growth the nervous system is modified in part by increasing numbers of individual subtypes in accordance with increasing body size.

5. Discussion

5.1. Neuronal subtype specification is stereotyped in number, location, and neurite projection patterns in Nematostella

The *Nematostella* nervous system is often described as a diffuse nerve net that has minimal reproducible architecture from animal to animal. However, there are examples of stereotypic neuronal structures present in several cnidarian species, but these structures have not been examined at the level of the individual neuron. Here we examine a small number of neurons that express *NvLWamide-like*, which allows

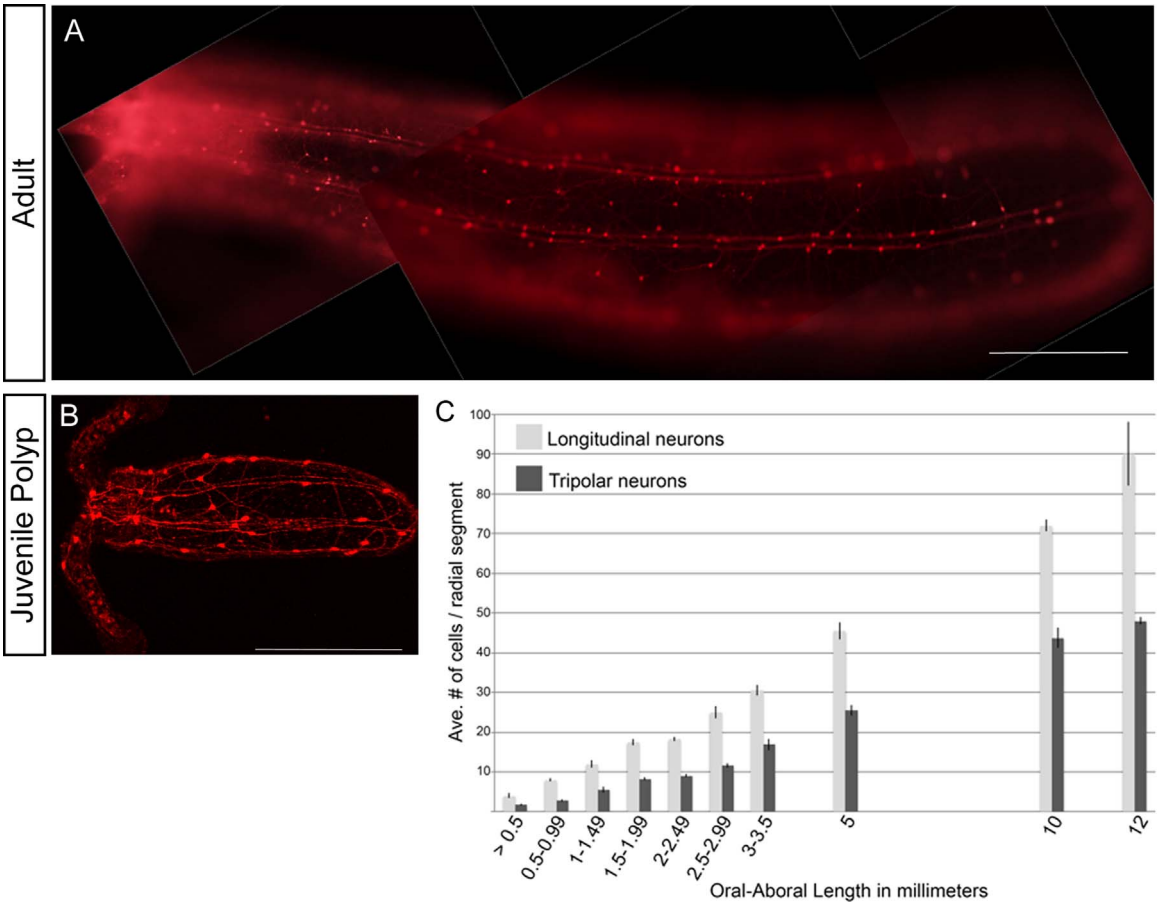

Fig. 7. Comparison of NvLWamide-like::mCherry neurons present in juveniles and adults. (A) Adult Nematostella has a significant increase in the number of NvLWamide-like::mCherry positive neurons compared to the juvenile polyp, but no new neuronal NvLWamide-like positive subtypes are observed. (B) NvLWamide-like::mCherry positive neurons in the juvenile polyp. In both animals oral end is to the left. Scale bars = 200 μm. mCherry expression in A and B highlights NvLWamide-like positive neurons in live animals relaxed in 3.57% $MgCL_2$ in 1/3 × ASW. (C) Graph of the average number of longitudinal (light grey) and tripolar (dark grey) neurons present in each radial segment in animals of different lengths. Juvenile polyps are contained in the > 0.5 category. We were able to score two radial segments in each animal. N = 13, 5, 8, 14, 14, 9, 9, 4, 2, 1 for > 0.5–12 mm respectively.

Table 1
Quantification of NvLWamide-like::mCherry cells in 12–14 day old juvenile polyps. The average number of NvLWamide-like::mCherry positive cells was quantified either per animal (pharyngeal), per mesentery, per tentacle, or per radial segment (tripolar and quadripolar).

Neuronal Subtype	Average	Stdev	SEM	n
Pharyngeal	25.9	6.09	1.39	19 animals
Mesentery	2.79	1.13	0.26	19 mesenteries
Longitudinal	4.85	1.01	0.17	34 radial segments
Tentacular	2.89	1.71	0.19	82 tentacles
Tripolar	1.4	0.82	0.11	52 radial segments
Quadripolar	0.23	0.43	0.06	52 radial segments
Tri/Quad	1.63	0.95	0.13	52 radial segments

us better visualize potential organization masked when observing the nerve net in its entirety.

We observed reproducible neuronal subtypes: longitudinal, tripolar, quadripolar, pharyngeal, tentacular, and mesentery labeled by the *NvLWamide-like::mCherry* transgene. Through the comparison of multiple animals at the end of development we found that the locations, number, and neurite projections patterns of neuronal subtypes were consistent across multiple animals. The number of neurons for each cell type was not exact (Table 1), suggesting that development is not as stereotyped as that observed in *Drosophila* ventral nerve chords, which have essentially no variation (Schmid et al., 1999). However the reproducibility of neuronal subtype development across animals suggests that what appears as an "irregular" nerve net when viewed in its entirety, likely contains unappreciated levels of organization. Further characterization of the development and structure of other cnidarian developmental model nerve nets such as *Clytia hemisphaerica* and *Hydractinia* is necessary to determine if stereotypy in nervous system development is a widespread phenomenon in cnidarian neurogenesis.

We further demonstrated that developmentally specified neural subtypes persist throughout the adult stage. However, the number of neurons in each subtype increases, and in the case of the longitudinal and ectodermal tripolar/quadripolar neurons there is a correlation between the numbers of neural bodies and body column length (Fig. 7C). The number of pharyngeal, mesentery, and tentacular neurons also increased, but were difficult to count reliably in adult animals. Together our data suggest specific neuronal subtypes and their neurite projection patterns are established during development, resulting in the basic scaffold for adult neural architecture. We hypothesize that the adult nerve net is generated by modifying the juvenile polyp nervous system primarily by increasing the number of neurons for each subtype.

Taken together, these data imply that the organization as a whole of cnidarian nerve nets is more stereotyped than previously appreciated. Recent work in *Hydra* identified non-overlapping neural networks responsible for regulating different behaviors (Dupre and Yuste, 2017). It stands to reason that some level of developmental coordination underlies reproducible construction of those networks, but the developmental basis of nerve net construction is not yet described in any cnidarian. Our data implies that subtype patterning programs result in reproducible neurite projection patterns that minimally bias particular

neurons to synapse with each other creating reproducible networks, and highlight the potential for *Nematostella* as a system to dissect the developmental basis of cnidarian neural networks.

5.2. Putative functions of subtypes expressing NvLWamide-like

We hypothesize that the tripolar, quadripolar, many of the tentacular and pharyngeal neurons are likely sensory neurons. They are all present in the ectoderm or ectodermal-derived structures and have a cell body that spans the depth of the epithelial layer. The morphology of their soma is also consistent with previously predicted ectodermal sensory neurons (Marlow et al., 2009; Nakanishi et al., 2012). In fact, it is possible that tripolar, quadripolar, and tentacular neurons are all the same neuronal subtype, but they reside in different locations and have slightly varying projection patterns.

Mesentery and longitudinal neurons likely function as interneurons. Their projections fasciculate into either the mesentery or the previously described longitudinal neural tracts, respectively (Marlow et al., 2009; Nakanishi et al., 2012). The longitudinal tracts contain a large number of neuronal projections, and are connected by commissural like structures (Supplemental Fig. 4), which is consistent with a neuropil-like structure. Alternatively the positioning of the longitudinal and mesentery neurons could also reflect a role in contraction of myoepithelial cells, as there is some evidence for LWamide family neuropeptides inducing muscle contractions in *Hydra* (Takahashi et al., 1997). We currently favor the hypothesis that the longitudinal neurons are interneurons because they are likely buried in the longitudinal tracts and not adjacent to the myoepithelial cells. However, we remain agnostic in regards to either hypothesis for the mesentery neurons.

5.3. Development and patterning of the neuronal subtypes

The developmental mechanism(s) that pattern the *NvLWamide-like* subtypes remains unknown. Some evidence suggests that in *Nematostella* regional patterning likely interacts with neural programs to generate specific neural subtypes (Layden et al., 2012; Leclère et al., 2016; Marlow et al., 2013; Watanabe et al., 2014). This is most evident in the requirement of proper directive axis formation to pattern asymmetrically distributed GLWamide+ neurons (Watanabe et al., 2014), and in the expression of neural markers in the apical tuft, which requires proper establishment and maintenance of oral-aboral patterning programs (Leclère et al., 2016; Sinigaglia et al., 2015, 2013). Additional work has shown that regional boundaries with distinct gene expression profiles are established along the oral-aboral axis, which could be integrated into the generic neural patterning mechanisms previously identified to generate specific neural subtypes (Kusserow et al., 2005; Marlow et al., 2013). The tissue layer in which the neural cell resides and the temporal window in which the neural progenitor is born are additional factors that may contribute to neural subtype specification. To date our understanding of the temporal patterning in *Nematostella* is poor, but future work aimed at understanding how distinct neural fates arise should not ignore this component.

Our data also speak to the cellular mechanisms related to generating the appropriate number of each neural subtype from neural progenitor cells. Vertebrate neurogenesis occurs by overproducing neurons and neurons that fail to properly synapse with target cells do not survive. *Drosophila* ventral nerve cords form from hardwired neuroblasts that generate neural subtypes in an exact lineage so that there is essentially zero variability in regards to neural number between animals (Schmid et al., 1999). *Nematostella* neurogenesis appears to be in between these approaches. We observe stereotyped numbers of each neural subtype, but typically there is a 1–2 cell number variability for each cell type between animals, and even between radial segments in the same animal. These data suggest that neural progenitor lineages are not hardwired. Additionally, with the exception of the reduction in ectodermal *NvLWamide-like* positive cells in the aboral ectoderm, it does not appear that there is a massive over production of *NvLWamide-like* neurons that then compete for a limited number of targets.

NvLWamide-like::mCherry expression describes a subset of the *Nematostella* nervous system. To fully understand the molecular and cellular programs that drive the development of diverse neural cell types, it will be necessary to generate new transgenic lines that identify additional subtypes of neurons in the *Nematostella* nervous system. The distinct neural subtypes will then need to be mapped to unequivocally establish their spatiotemporal origin during development, as well as the molecular program that specifies each cell type. Once we better understand the molecular programs controlling development of various neural cell types in cnidarians, we will then be poised to ask questions regarding the relationship of bilaterian nervous systems to some or all of the cnidarian nerve net.

Acknowledgements

We would like to acknowledge Uli Technau (University of Vienna, Austria) and Fabian Rentzsch (University of Bergen, Norway) for providing the pNvT vector necessary to generate the *NvLWamide::mCherry* transgene and the *Nvelav1::mOrange* transgenic strain. This research did not receive any specific grant from funding agencies in the public, commercial, or not-for-profit sectors.

Appendix A. Supporting information

Supplementary data associated with this article can be found in the online version at doi:10.1016/j.ydbio.2017.08.028.

References

Anderson, P.A., Thompson, L.F., Moneypenny, C.G., 2004. Evidence for a common pattern of peptidergic innervation of cnidocytes. Biol. Bull., 141–146.
Arendt, D., Denes, A.S., Jekely, G., Tessmar-Raible, K., 2008. The evolution of nervous system centralization. Philos. Trans. R. Soc. B: Biol. Sci. 363, 1523–1528. http://dx.doi.org/10.1016/S0925-4773(00)00298-7.
Babonis, L.S., Martindale, M.Q., Ryan, J.F., 2016. Do novel genes drive morphological novelty? An investigation of the nematosomes in the sea anemone Nematostella vectensis. BMC Evol. Biol., 1–22. http://dx.doi.org/10.1186/s12862-016-0683-3.
Darling, J.A., Reitzel, A.R., Burton, P.M., Mazza, M.E., Ryan, J.F., Sullivan, J.C., Finnerty, J.R., 2005. Rising starlet: the starlet sea anemone, Nematostella vectensis. Bioessays 27, 211–221, (doi:10.1002/bies.20181).
Donaldson, S., Mackie, G.O., Roberts, A., 1980. Preliminary observations on escape swimming and giant neurons in Aglantha Digitale (Hydromedusae: Trachylina). Can. J. Zool. 58, 549–552.
Dunn, C.W., Hejnol, A., Matus, D.Q., Pang, K., Browne, W.E., Smith, S.A., Seaver, E., Rouse, G.W., Obst, M., Edgecombe, G.D., Sørensen, M.V., Haddock, S.H.D., Schmidt-Rhaesa, A., Okusu, A., Kristensen, R.M., Wheeler, W.C., Martindale, M.Q., Giribet, G., 2008. Broad phylogenomic sampling improves resolution of the animal tree of life. Nature 452, 745–749. http://dx.doi.org/10.1038/nature06614.
Dupre, C., Yuste, R., 2017. Non-overlapping neural networks in Hydra vulgaris. Curr. Biol. 27, 1085–1097. http://dx.doi.org/10.1016/j.cub.2017.02.049.
Fritzenwanker, J.H., Technau, U., 2002. Induction of gametogenesis in the basal cnidarian Nematostella vectensis (Anthozoa). Dev. Genes Evol. 212, 99–103. http://dx.doi.org/10.1007/s00427-002-0214-7.
Galliot, B., Quiquand, M., Ghila, L., de Rosa, R., Miljkovic-Licina, M., Chera, S., 2009. Origins of neurogenesis, a cnidarian view. Dev. Biol. 332, 2–24. http://dx.doi.org/10.1016/j.ydbio.2009.05.563.
Ghysen, A., 2003. The origin and evolution of the nervous system. Int. J. Dev. Biol. 47, 555–562.
Grimmelikhuijzen, C.J., Spencer, A.N., 1984. FMRFamide immunoreactivity in the nervous system of the medusa Polyorchis penicillatus. J. Comp. Neurol., 361–371.
Hand, C., Uhlinger, K.R., 1992. The Culture, Sexual and Asexual Reproduction, and Growth of the Sea Anemone *Nematostella vectensis*. Biol. Bull. 182, 169–176.
Hartenstein, V., Stollewerk, A., 2015. The evolution of early neurogenesis. Dev. Cell 32, 390–407. http://dx.doi.org/10.1016/j.devcel.2015.02.004.
Hejnol, A., Obst, M., Stamatakis, A., Ott, M., Rouse, G.W., Edgecombe, G.D., Martinez, P., Baguna, J., Bailly, X., Jondelius, U., Wiens, M., Muller, W.E.G., Seaver, E., Wheeler, W.C., Martindale, M.Q., Giribet, G., Dunn, C.W., 2009. Assessing the root of bilaterian animals with scalable phylogenomic methods. Proc. R. Soc. B: Biol. Sci. 276, 4261–4270. http://dx.doi.org/10.1006/jtbi.1999.0999.
Hejnol, A., Rentzsch, F., 2015. Neural nets. Curr. Biol. 25, R782–R786. http://dx.doi.org/10.1016/j.cub.2015.08.001.

Koizumi, O., Hamada, S., Minobe, S., Hamaguchi-Hamada, K., Kurumata-Shigeto, M., Nakamura, M., Namikawa, H., 2015. The nerve ring in cnidarians: its presence and structure in hydrozoan medusae. Zoology 118, 79–88. http://dx.doi.org/10.1016/j.zool.2014.10.001.

Koizumi, O., Sato, N., Goto, C., 2004. Chemical anatomy of hydra nervous system using antibodies against hydra neuropeptides: a review. Hydrobiologia, 41–47.

Kusserow, A., Pang, K., Sturm, C., Hrouda, M., Lentfer, J., Schmidt, H.A., Technau, U., Haeseler, von, A., Hobmayer, B., Martindale, M.Q., Holstein, T.W., 2005. Unexpected complexity of the Wnt gene family in a sea anemone. Nature 433, 156–160. http://dx.doi.org/10.1038/nature03158.

Layden, M.J., Boekhout, M., Martindale, M.Q., 2012. Nematostella vectensis achaete-scute homolog NvashA regulates embryonic ectodermal neurogenesis and represents an ancient component of the metazoan neural specification pathway. Development 139, 1013–1022. http://dx.doi.org/10.1242/dev.073221.

Layden, M.J., Johnston, H., Amiel, A.R., Havrilak, J., Steinworth, B., Chock, T., Röttinger, E., Martindale, M.Q., 2016a. MAPK signaling is necessary for neurogenesis in Nematostella vectensis. BMC Biol., 1–19. http://dx.doi.org/10.1186/s12915-016-0282-1.

Layden, M.J., Martindale, M.Q., 2014. Non-canonical Notch signaling represents an ancestral mechanism to regulate neural differentiation. Evodevo 5, 1–14. http://dx.doi.org/10.1186/2041-9139-5-30.

Layden, M.J., Rentzsch, F., Röttinger, E., 2016b. The rise of the starlet sea anemone Nematostella vectensis as a model system to investigate development and regeneration. WIREs Dev. Biol., 1–21. http://dx.doi.org/10.1002/wdev.222.

Leclère, L., Bause, M., Sinigaglia, C., Steger, J., Rentzsch, F., 2016. Development of the aboral domain in Nematostella requires β-catenin and the opposing activities of Six3/6 and Frizzled5/8. Development 143, 1766–1777. http://dx.doi.org/10.1242/dev.120931.

Mackie, G.O., 2004. Central neural circuitry in the jellyfish aglantha. Neurosignals 13, 5–19. http://dx.doi.org/10.1159/000076155.

Marlow, H., Matus, D.Q., Martindale, M.Q., 2013. Ectopic activation of the canonical wnt signaling pathway affects ectodermal patterning along the primary axis during larval development in the anthozoan Nematostella vectensis. Dev. Biol. 380, 324–334. http://dx.doi.org/10.1016/j.ydbio.2013.05.022.

Marlow, H.Q., Srivastava, M., Matus, D.Q., Rokhsar, D., Martindale, M.Q., 2009. Anatomy and development of the nervous system of Nematostella vectensis, an anthozoan cnidarian. Dev. Neurobiol. 69, 235–254. http://dx.doi.org/10.1002/dneu.20698.

Nakanishi, N., Renfer, E., Technau, U., Rentzsch, F., 2012. Nervous systems of the sea anemone Nematostella vectensis are generated by ectoderm and endoderm and shaped by distinct mechanisms. Development 139, 347–357. http://dx.doi.org/10.1242/dev.071902.

Putnam, N.H., Srivastava, M., Hellsten, U., Dirks, B., Chapman, J., Salamov, A., Terry, A., Shapiro, H., Lindquist, E., Kapitonov, V.V., Jurka, J., Genikhovich, G., Grigoriev, I.V., Lucas, S.M., Steele, R.E., Finnerty, J.R., Technau, U., Martindale, M.Q., Rokhsar, D.S., 2007. Sea anemone genome reveals ancestral eumetazoan gene repertoire and genomic organization. Science 317, 86–94. http://dx.doi.org/10.1126/science.1139158.

Rentzsch, F., Fritzenwanker, J.H., Scholz, C.B., Technau, U., 2008. FGF signalling controls formation of the apical sensory organ in the cnidarian Nematostella vectensis. Development 135, 1761–1769. http://dx.doi.org/10.1242/dev.020784.

Rentzsch, F., Layden, M., Manuel, M., 2016a. The cellular and molecular basis of cnidarian neurogenesis. WIREs Dev. Biol., 1–19, (doi:10.1002/wdev.257).

Rentzsch, F., Layden, M., Manuel, M., 2016b. The cellular and molecular basis of cnidarian neurogenesis. WIREs Dev. Biol. 6, e257, (19. doi:10.1002/wdev.257).

Richards, G.S., Rentzsch, F., 2015. Regulation of Nematostella neural progenitors by SoxB, Notch and bHLH genes. Development 142, 3332–3342. http://dx.doi.org/10.1242/dev.123745.

Richards, G.S., Rentzsch, F., 2014. Transgenic analysis of a SoxB gene reveals neural progenitor cells in the cnidarian Nematostella vectensis. Development 141, 4681–4689. http://dx.doi.org/10.1242/dev.112029.

Roberts, A., Mackie, G.O., 1980. The giant axon escape systme of a hyrdrozoan medusa, Aglantha Digitale. J. Exp. Biol. 84, 303–318.

Saina, M., Genikhovich, G., Renfer, E., Technau, U., 2009. BMPs and chordin regulate patterning of the directive axis in a sea anemone. Proc. Natl. Acad. Sci. USA 106, 18592–18597. http://dx.doi.org/10.1073/pnas.0900151106.

Schmid, A., Chiba, A., Doe, C.Q., 1999. Clonal analysis of Drosophila embryonic neuroblasts: neural cell types, axon projections and muscle targets. Development 126, 4653–4689.

Sinigaglia, C., Busengdal, H., Leclère, L., Technau, U., Rentzsch, F., 2013. The bilaterian head patterning gene six3/6 controls aboral domain development in a cnidarian. PLoS Biol. 11, e1001488. http://dx.doi.org/10.1371/journal.pbio.1001488.

Sinigaglia, C., Busengdal, H., Lerner, A., Oliveri, P., Rentzsch, F., 2015. Molecular characterization of the apical organ of the anthozoan Nematostella vectensis. Dev. Biol. 398, 120–133. http://dx.doi.org/10.1016/j.ydbio.2014.11.019.

Takahashi, T., Muneoka, Y., Lohman, J., Lopez de Haro, M., Solleder, G., Bosch, T.C.G., David, C.N., Bode, H.R., Koizumi, O., Shimizu, H., Masayuki, H., Fujisawa, T., Sugiyama, T., 1997. Systematic isolation of peptide signal molecules regulating development in hydra: LWamide and PW families. Proc. Natl. Acad. Sci. USA 94, 1241–1246.

Watanabe, H., Fujisawa, T., Holstein, T.W., 2009. Cnidarians and the evolutionary origin of the nervous system. Dev., Growth Differ. 51, 167–183. http://dx.doi.org/10.1111/j.1440-169X.2009.01103.x.

Watanabe, H., Kuhn, A., Fushiki, M., Agata, K., Ozbek, S., Fujisawa, T., Holstein, T.W., 2014. Sequential actions of β-catenin and Bmp pattern the oral nerve net in Nematostella vectensis. Nat. Commun. 5, 5536. http://dx.doi.org/10.1038/ncomms6536, (14).

Wolenski, F.S., Layden, M.J., Martindale, M.Q., Gilmore, T.D., Finnerty, J.R., 2013. Characterizing the spatiotemporal expression of RNAs and proteins in the starlet sea anemone, Nematostella vectensis. Nat. Protoc. 8, 900–915. http://dx.doi.org/10.1038/nprot.2013.014.